NLUAstro 2, 1-15 (2020) Notices of Lancaster University Astrophysics PHYS369: Astrophysics Group project

An analysis of the local causes and effects of AGN produced jets in galaxies at z ∼ 2 − 3.5 ⋆

Georgia Stevens[1], Jim Warner[1], Daniel Head[1], Stephen Griffin[1], Alaister Foster[1], & David Sobral[1]†
[1] *Department of Physics, Lancaster University, Lancaster, LA1 4YB, UK*

Accepted 18 June 2020. Received 2 June 2020; in original form 19 March 2020

ABSTRACT

We investigate the radio, X-Ray and far-infrared properties of active galactic nuclei (AGN) with strong radio jets at $2.2 < z < 3.5$ in the COSMOS field and compare them to AGN without obvious radio jets at similar redshift. We identify 4 jet producing AGNs in the SC4K sample of distant Lyman-α emitting sources and 8 in the VLA radio catalogue, with 2 sources being represented in both, implying a jet fraction of 0.13±0.04% in Lyα emitters and 0.71±0.08% in the general radio-selected population. We find an average radio luminosity for the jets of $2.27 \pm 0.01 \times 10^{25}$ W Hz^{-1} in the 3GHz band and $3.10 \pm 0.01 \times 10^{25}$ W Hz^{-1} in the 1.4GHz band. We find that the average accretion rate of the AGNs with jets is $0.141^{+0.078}_{-0.016}$ M$_\odot$yr^{-1} which is lower than the average of the radio AGN without jets, of $0.271^{+0.091}_{-0.019}$M$_\odot$yr^{-1}. The star formation rate based on the far-infrared is found to be higher for AGN without jets of 274±8.14M$_\odot$yr^{-1} and to be a third of that value for AGN with jets 92.0±2.11M$_\odot$yr^{-1}. All the jet producing AGNs we found at z < 3 had an X-ray hardness > 0 and average of 0.41±0.21, higher than the average for AGN without jets of 0.14±0.47. We conclude that the presence of jets inhibit the AGN's activity, due to the large size and luminosity of jets, the energy and matter distributions are altered in such a way that the galaxy's SFR and BHAR are impacted noticeably, agreeing with previous research and findings.

Key words: galaxies, AGN, supermassive black holes, relativistic jets.

1 INTRODUCTION

Supermassive black holes (SMBHs) are believed to be found at the nucleus of every galaxy and to have masses in the range of 10^6 - 10^{10} M$_\odot$. Previous research shows a strong correlation between the SMBH and the properties of the galaxy which suggests that SMBHs heavily influence galaxy formation and evolution and vice versa (Narayan & McClintock 2013). There are several theories to explain the formation of SMBHs including the hydrodynamical collapse of protogalactic gas clouds to form black hole seeds from which SMBHs can grow (Loeb & Rasio 1994). Other studies have suggested that some of the very first stars (known as Population III stars) may have been responsible for the formation of large populations of intermediate mass black holes (IMBHs) as documented in Madau & Rees (2001). The implications of the detection of intermediate mass black holes in the formation of SMBHs is discussed in Mezcua (2017) and Mezcua et al. (2018) with these IMBHs believed to act as the seeds before accretion processes form SMBHs.

Active galactic nuclei (AGNs) are thought to be the result of an active SMBH. They contain an accretion disk and this is believed to be formed from when the gas surrounding the SMBH cools in an equatorial plane which is oriented perpendicular to the axis of rotation of the SMBH due to its rapid spinning (see Blandford et al. 2019, and references therein). The gas within this thin accretion disk can then spiral inwards towards the SMBH due to magnetic torques the gas sustains due to magnetorotational instabilities arising due to the variation in angular velocity with distance to the centre of rotation of the accretion disk as demonstrated in Balbus & Hawley (1998). The radiation that is trapped by the inflowing gas and the radiation pressure causes this disk to thicken and form a torus shape which is believed to contribute to the collimation of highly relativistic streams of matter (see Abramowicz & Fragile 2013, and references therein). These streams of matter are known as jets and they

⋆ Based on SC4K (Sobral et al. 2018) and the VLA radio catalogue (Smolčić et al. 2017), with observations obtained by the VLA, *Chandra*, *HST*, Subaru and *Spitzer*.
† PHYS369 supervisor

are ejected from the accreting SMBH. Allen et al. (2006) have found that these jets can encourage a feedback mechanism and can influence the properties of the galaxy.

It is possible to detect the processes that occur within the AGN through the emission of radiation in both the X-ray and radio bands. The accreting SMBH can convert gravitational binding energy into intense radiation (McKinney et al. 2013) which is emitted from the AGN making them highly luminous. This is demonstrated further by Calhau et al. (2020) as they find that the AGN population of Lyman-α emitters between 2<z<6 has Lyα luminosity tracing the black hole accretion rate. Furthermore, X-ray radiation can be used to trace the activity of the SMBH from inverse-Compton scattering and Bremsstrahlung processes. On the other hand, radio emissions are from relativistic electrons spiralling along a uniform magnetic field emitting radiation with a characteristic frequency known as synchotron radiation (Blandford et al. 2019) and this can be detected in jets and from within the AGN.

Jet formation whilst still a mystery is thought to occur through a number of complex physical processes. The interaction between the SMBH and the accretion disk during the Blandford-Znajek process as described in Blandford & Znajek (1977) involves the magnetic field sustained by the matter within the accretion disk interacting with the ergosphere of the rotating SMBH. The ergosphere spans the event horizon at the poles and the Schwarzschild radius in the equatorial area. It is possible for mass and energy to be extracted from this region which can then be used in jet formation, but the efficiency of this mechanism is unknown (Ghisellini et al. 2009). However, Blandford & Znajek (1977) has come under criticism from Ghosh & Abramowicz (1997) for over-estimating the strength of the magnetic field threading the black hole ergosphere. Alternatively, a mechanism known as the Penrose mechanism (Penrose & Floyd 1971) can also be used to explain the extraction of energy from the rotation of a black hole in order to accelerate the jet material. Despite this process having similarities to the Blandford-Znajek mechanism in extracting the rotational energy from the black hole within the ergosphere, it does not involve magnetism. Instead, matter can enter the ergosphere and break apart with some matter escaping the ergosphere with more energy than it entered with whilst still conserving momentum. We will investigate the relationship between the accretion rate and jet formation to determine whether this supports the theories of Blandford & Znajek (1977) and Penrose & Floyd (1971) in the mechanism for the acceleration of jets.

In contrast to the puzzle around the origin of their formation, jets are known to form with a predictable structure known as the spine-sheath model which has a highly relativistic inner 'spine' and a mildly relativistic 'sheath' (King et al. 2015). There are two main types of jets which are classified based on the Fanaroff-Riley (FR) class of the radio source - a system clarified within Fanaroff & Riley (1974). These sources are known to produce distinctly different jets known as FR-I and FR-II. These jets differ in their morphology with FR-II jets having lobes with brighter edges with bright hotspots whereas FR-I jets have lobes with darker edges. Their particle composition is also known to differ with FR-I jets mostly composed of an electron-positron plasma in contrast to FR-II jets which are composed of an electron-proton plasma (e.g. Croston et al. 2018; Celotti et al. 1997). Therefore, if there was any bias towards a particular jet type this would result in jets with only specific properties being detected. In order to detect the presence of jets from an AGN it has been important to understand the background to jet formation as well as jet classification. This has allowed us to visually categorise the jet sources that we detect and allow us to come to a conclusion about the possibility of bias towards a particular type of jet. It has enabled us to see that the class of jet can influence the luminosity measurements that we detect with FR-II jets being significantly more luminous than FR-I jets.

Another noticeable element of jet structure is the collimation of jets in which a contribution was made by Blandford & Payne (1982). The model constructed to explain jet collimation suggests the presence of a poloidal magnetic field acting on material within the accretion disk and if this magnetic field is aligned at an angle of less than 60° to the rotation axis then it is energetically favourable for to be flung from the accretion disk. Material has in the meantime been accelerated due to the centrifugal force experienced until it reaches the Alfven surface in which the magnetic energy density is equivalent to the kinetic energy density (Livio 1997). Beyond this point the material can then be collimated by 'hoop stresses' due to the effect of inertia on the gas causing it to lag behind the rotation of the magnetic field (Spruit 1996). This process only occurs when the radius of the central object is much smaller than the radius of the disk such as in AGNs as Livio (1997) demonstrated and from these expected sizes a minimum bound can be put on the opening angle of ≈ 0.01. The small opening angle in consistent with the idea of powerful and highly collimated jets. We will use the theory of highly collimated jets proposed by Blandford & Payne (1982) and the estimate of the lower bound for their opening angle (Livio 1997) in a jet flux with distance calculation in order to estimate the radiative effects of jets and the impacts this can have on their environment.

We have noticed that there is often a significant amount of variation when it comes to the fraction of jetted AGN. Padovani (2017) suggests that the fraction of jetted AGN in the bright radio band (when radio flux $> 1mJy$) is less than 10% whereas suggest that the dimmer radio band mainly consists of non-jetted AGN. On the other hand, Torres-Albà et al. (2020) assumes that the jetted fraction (for the brightest AGN) is almost 1 when calculating the contribution of AGN to re-ionization at $z \approx 6$. Therefore it appears there is significant variation on the fraction of AGN that appear to be jetted even in the bright radio band. During this work we will examine the jetted fractions of AGN within the range $2,2 < z < 3.5$ in both the SC4K dataset (Sobral et al. 2018) and the VLA radio catalogue Smolčić et al. (2017) to observe how this jetted fraction varies, if at all, in comparison to previous studies.

We will also observe the dimmer radio band to observe if our jet fractions agree with the aforementioned conclusions made by Padovani (2017). In this study we aim to provide a detailed comparison as well as examine some of the potential causes of jet formation. Not only will we examine the theory proposed by Padovani (2017) in the jetted fractions with varying radio flux of the AGN. In addition, we investigate the impacts that jets can have on their surrounding environment such as the impact on exoplanet habitability and

the star formation rate of the AGN. Ultimately, this work will provide a greater understanding of the factors that are involved in jet formation and allow us to see the properties of the galaxy that jets can affect, useful for predicting the evolution of the galaxy.

This paper is organised as follows: Section 2 describes the sample and data that we have used within this work. Section 3 details the methods we have used for jet detection in the X-ray and radio as well as calculating the properties of the AGNs including star-formation rate (SFR) and black hole accretion rate (BHAR). Section 4 and 5 present the results of the jetted and non-jetted AGN sources and discuss what is observed. Finally, our conclusions from this paper are presented in Section 6. In this work we use flat cosmology: $H_0 = 70$ km s^{-1}Mpc^{-1}, $\Omega_M = 0.3$ and $\Omega_\Lambda = 0.7$.

2 DATA AND SAMPLE

2.1 SC4K Lyα emitters

Calhau et al. (2020) use a large sample of LAEs selected over a redshift range of $2 < z < 6$ in the COSMOS field (SC4K: Sobral et al. 2018). SC4K also includes the CALYMHA COSMOS sample at z=2.2 (Sobral et al. 2017), with Hα coverage from HiZELS (Geach et al. 2008; Sobral et al. 2009, 2013). The LAEs were detected using a compilation of 16 narrow and medium band (MB) data taken with the Subaru and the Isaac Newton Telescopes. Sobral et al. (2018) consider only the sources covered by Chandra COSMOS Legacy (Civano et al. 2016), for a total of 3,700 sources. We refer to Sobral et al. (2018) for the full selection criteria and further details regarding the SC4K LAEs. Calhau et al. (2020) uses the 3 GHz VLA data to further probe the existence of radio-active AGN over a larger area, by removing radio AGN and obtaining deep radio stacks, radio data allowed a dust-independent determination of the SFRs of SC4K LAEs to give us the data table of over 3,900 sources. We can see that 3,091 of the sources are within the redshift range $2.2 < z < 3.5$, as shown by Figure 1, so we use this set of data as a more defined sample of sources.

2.2 Radio data: 1.4GHz and 3GHz VLA-COSMOS

The VLA-COSMOS Survey (Schinnerer et al. 2004; Schinnerer et al. 2007; Bondi et al. 2008; Schinnerer et al. 2010) used the National Radio Astronomy Observatory's Very Large Array (VLA) to conduct deep, wide-field imaging with ~ 1.5" resolution at 1.4 GHz continuum of the 2 deg^2 COSMOS field. The data reaches down to a 1σ sensitivity of about 11 μJy beam^{-1}, leading to Bondi et al. (2008) presenting a catalog of roughly 3600 radio sources. The VLA's 3 GHz COSMOS Large Project covers the entirety of the COSMOS field at a deeper average sensitivity of 2.3 μJybeam^{-1} and also at a higher spatial resolution, with an average beam-width of 0.75". The observations and data reduction details can be found in Smolčić et al. (2017) including a catalogue of over 10,000 radio sources, that we will be analysing.

The radio sources are spread over a wide range of redshifts, so we took a subset of z = 2.2 to z = 3.5 as that is the redshift band where the majority of the LAE's from the SC4K catalogue are. After visually examining some of the given sources, we also implemented a minimum brightness cut of 10 μ Jy beam^{-1} such that when we come to examine the sources, they will be visible and identifiable. From over 10,000 radio sources in Smolčić et al. (2017) this gave us 1,156 sources for us to examine further.

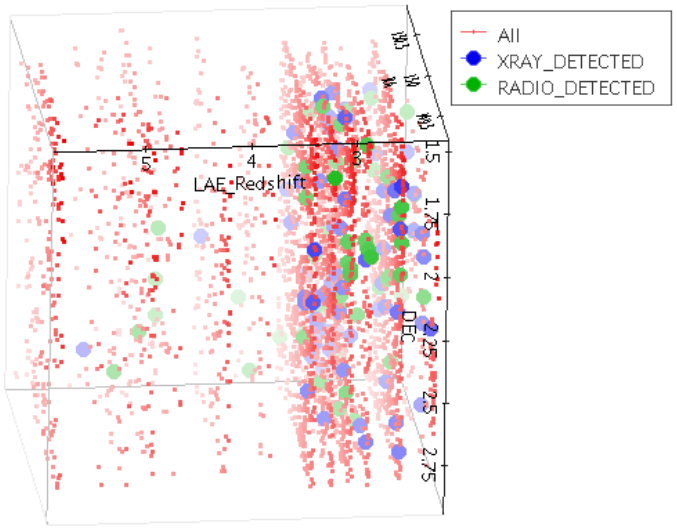

Figure 1. Plot of our Lyman-α emitting sources with respective redshifts and R.A and Dec. co-ordinates. Sources with strong radio/X-ray emissions are marked green/blue respectively, and can be seen to cluster about the $2.2 < z < 3.4$ range.

2.3 X-ray data: *Chandra* COSMOS-Legacy

The Chandra COSMOS-Legacy survey (Elvis et al. 2009; Civano et al. 2016) covers the COSMOS field (e.g. Scoville et al. 2007; Capak et al. 2007) over a total area of 2.2 deg^2. The survey has an exposure time of 150 ks px^{-1} in the central 1.5 deg^2 and between 50 ks px^{-1}to 100 ks px^{-1} in the external regions. The flux limit of the survey, as defined by the source catalogue (Civano et al. 2016) is 8.9×10^{-16} erg s^{-1}cm^{-2} for the full band (0.5-7keV), 2.2×10^{-16}erg s^{-1}cm^{-2} for the soft band (0.5-2keV) and 1.5×10^{-15}erg s^{-1}cm^{-2} for the hard band (2-7keV). The deep X-ray data allow us to track X-ray emission from processes like Bremsstrahlung and inverse-Compton scattering, and thus to identify AGN X-ray emission when observing galaxies with jets.

2.4 Infrared data: *Spitzer/MIPS* 24μm COSMOS

As described and used in Le Floc'h et al. (2009), the COSMOS field was observed at 24 μm with the MIPS instrument onboard *Spitzer* as part of two General Observer programs (PI: D. Sanders). The first observations (GO2, PID 20070) were carried out in 2006 January with the MIPS medium scan mode and two scan passes per sky pixel. As described in more detail by Sanders et al. (2007), this shallow imaging covered a total area of approximately 4 deg^2 centered on COSMOS, with a median integration time of 80s per pixel. This first program was also used to test in a small region

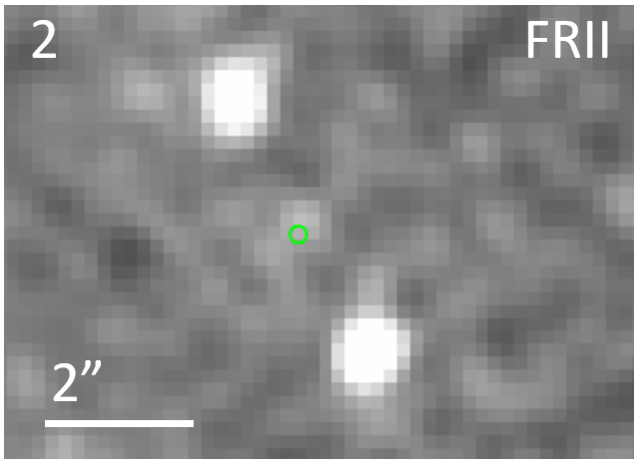

Figure 2. 3GHz radio image of SC4K-IA464-75921, one of our highest confidence jet sources. The small green circle in the center marks the radio detection from the AGN, and the two bright lobes distinctly show the ends of the jets. Following this, the X-ray and visible data are inspected to find where the source galaxy is in comparison to the jets, confirming the jets are from the selected source.

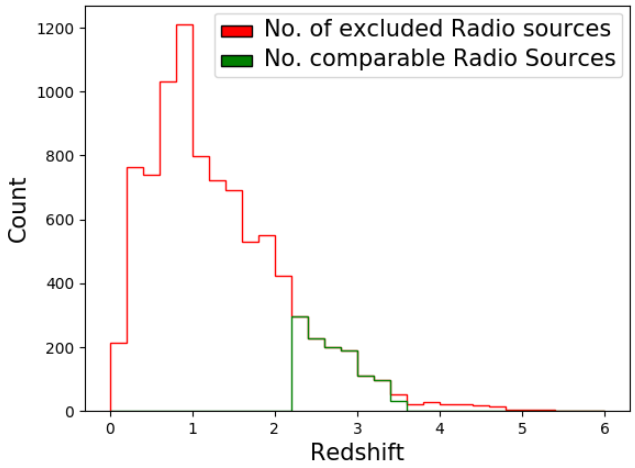

Figure 3. The number of sources from the VLA COSMOS catalogue showing the X-ray and radio detected AGN and the subset of the full Catalogue we selected for further analysis, through the redshift cut of $2.2 < z < 3.5$.

of the field the feasibility to improve the 24μm sensitivity with longer integrations despite the COSMOS mid-IR background being 2× higher than in other typical “cosmological” fields. Deeper imaging was performed in 2007 over the whole COSMOS field as part of a second program using the MIPS slow scan mode (GO3, PID 30143). These data yielded a second and independent 24μm coverage over a total area of 3 deg^2. Across the nominal 2 deg^2 of COSMOS, the combination of the GO2 and GO3 observations results in a median integration time of ∼3360 s per sky pixel. COSMOS-Cutouts at `https://irsa.ipac.caltech.edu/data/COSMOS/index_cutouts.html` with `http://mipsgal.ipac.caltech.edu/a_mipsgal.html` allows us to gain all Infrared data used in this report.

3 METHODOLOGY

Here we present the full methodology leading to all of the quantities that are explored in this paper. This includes X-ray, radio 1.4GHz and 3GHz and far infra-red (FIR) derived properties.

3.1 Identification of jet sources

The jets were identified by visually checking the SC4K (Sobral et al. 2018) and the larger VLA Cosmos (Smolčić et al. 2017) samples. From these we were able to successfully identify a total of ten viable sources we were confident were jets to investigate further, the method of such is described in the sections below.

3.1.1 SC4K dataset

To identify the jets we initially looked at every source in the SC4K catalogue in the 3GHz radio band to obtain a list of 48 sources that appeared to be potential jets. These 48 then underwent more rigorous observation in both radio frequencies, optical and infrared images (the infrared and optical images were obtained from `https://irsa.ipac.caltech.edu/data/COSMOS/index_cutouts.html`). This allowed us to come to the conclusion that a galaxy with a nearby bright spot in the 1.4GHz and 3GHz radio images and nothing visible in either optical or infrared images indicated the presence of the radio bulb of a jet, thereby indicating the presence of an FR-II type jet. An example is galaxy SC4K-IA464-75921, shown in Figure 2. From this process in the SC4K catalogue, we find 4 sources of jets, all FR-II classification. There is a high probability that this method had a bias towards detecting FR-II type jets as FR-I type jets do not have a radio bulb that makes them easily identifiable in the radio spectrum which we are investigating, which means our sample does not reflect a true distribution of jet morphologies that occur naturally, it only reflects the distribution of most observable.

3.1.2 VLA Radio Catalogue

The VLA COSMOS radio catalogue provided 1,156 sources within the range ($2.2 < z < 3.5$) as decided in Section 2.2. Figure 3 and Figure 4 demonstrate the cropped sample against the full catalogue (see Smolčić et al. 2017).

All sources were put through the same process as the SC4K sample where each suspected sources’ radio images in the 1.4GHz and 3GHz were compared to the optical and infrared images. We found 6 sources of jets, their ID’s are all listed in Table 1, of which 4 are FR-II and 2 are FR-I classifications.

3.2 Radio analysis

This section outlines how we utilised and ultimately analysed our VLA COSMOS dataset (see section 2.2) in order

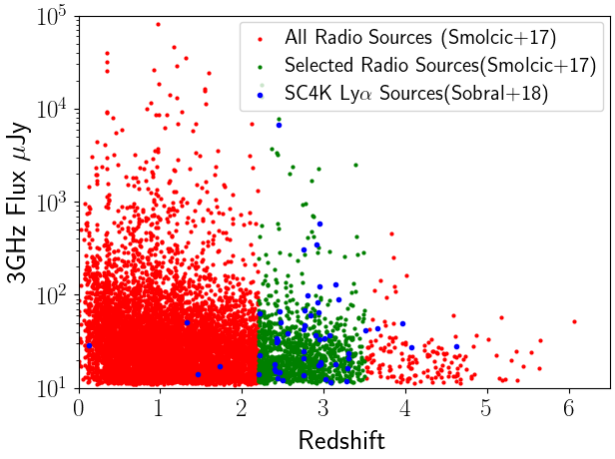

Figure 4. The 3 GHz flux of sources from the VLA Cosmos catalogue against their respective redshift with the selected subset of radio sources in green and the LAEs which were in both the VLA Cosmos and SC4K catalogues in blue.

to obtain the radio fluxes and therefore luminosities of the identified sources.

3.2.1 Radio Counts and Background Estimation

In the 1.4GHz and 3GHz radio bands, we determine the radio count of flux density in μJy beam^{-1} by placing custom individual apertures ranging from 1.4" (0.7" radius) to 4.6" (2.3" radius) such that the area covered by the aperture is centered on the jet lobe we are performing the measurement on (see Figure 6). We placed an aperture of 6" (3" radius) in the largest available space of the image to calculate the background count that was subtracted from the overall source flux being measured. The resolution of the 1.4GHz band is poorer than the 3GHz band, so on average larger apertures were used in this band such that we are fully confident the aperture placed covers and measures the entire jet in the image.

3.2.2 Radio Luminosity Estimation

Previous research (Calhau et al. 2020) apply an aperture correction to median match other catalogue fluxes (such as Bondi et al. 2008; Smolčić et al. 2017). While it was first necessary to convert our given sources' spectral flux density from Jansky to the correct unit of flux for this (W Hz^{-1}m^{-2}), we do not apply an aperture correction, as our apertures were of varying (but always measured) size, so we let this simply be our full radio flux (F_ν). We then estimate the radio luminosities of our sources as below:

$$L_\nu = \frac{4\pi d_L^2}{(1+z)^{\alpha+1}} F_\nu (\mathrm{W\ Hz^{-1}}) \quad (1)$$

The luminosity distance d_L, in meters here, was calculated in Topcat. F_ν is the flux at 1.4 GHz or 3 GHz and α is the radio spectral index. We assume that α = -0.8, as this is the characteristic spectral index of synchrotron radiation and the value typically found in AGN (as detailed in Delhaize et al. 2017).

3.3 X-ray analysis

X-ray are particularly useful in this area due to the inverse Compton effect within the accretion disk as documented in Haardt & Maraschi (1991). This causes the X-ray luminosity to scale proportionally with the BHAR, while also allowing the use of this luminosity to identify the presence of the AGN itself. By deducing and calculating many variables (e.g. radio and X-ray luminosity) related to our jet (and non-jet) sources, and controlling variables (such as redshift, hardness ratio, and ratio of Lyα emitters) where possible, we can best compare them in order to hopefully shed light on what may be critical in the formation of jets.

3.3.1 Source Detection

For our X-ray analysis we use a similar method to Calhau et al. (2020) and data from the COSMOS Legacy Survey (Civano et al. 2016). We transform the images into counts using the corresponding exposure maps. In this study we used 9 px (8.9") diameter circular apertures, centered on the location of each source. this allows us to extract the majority of the fluxes from the majority of the sources (~80% - see Civano et al. (2016)) without adding significant noise to the measurements. We still apply a final small aperture correction to assure we recover the full flux (see Section 3.3.3).

3.3.2 X-ray count and Background Estimation

To calculate the background counts, we took readings from 2000 randomly placed apertures spread over the region within a 100 by 100 pixel square centered on each source. The background apertures were placed in this region to provide a measure of the local background around each source instead of the background of the entire image. The total counts/s in each aperture is calculated and the median of the 2000 apertures is taken as the background, which is then subtracted from the net counts/s of the source.

The uncertainty is then measured by taking asymmetric errors. The upper and lower errors are defined as the 84th and 16th percentile of the backgrounds, respectively. A source is considered detected if the signal to noise ratio (S/N), which we define as the ratio between the net counts/s and the lower error of each source, is greater than or equal to 3.

3.3.3 X-ray flux estimation

We can estimate the equivalent flux corresponding to our X-ray counts using the following method, previously used and documented in Elvis et al. (2009) and Civano et al. (2016).

$$F_{X_0} = (\mathrm{counts/s}) \times CF \times 10^{-11} (\mathrm{ergs^{-1}cm^{-2}}) \quad (2)$$

As seen this involves multiplying our raw counts by both a factor of 10^{-11}, and the relevant conversion factor (CF) based off the average energy of the photons. The conversion factor accounts for the energy of the photons being detected and the efficiency of the detector in different bands. Various previous values for this factor have been published and utilised, but by averaging those from the aforementioned *Chandra* COSMOS surveys, C-COSMOS (Elvis et al. 2009) and *Chandra* Legacy (Civano et al. 2016), we obtain our

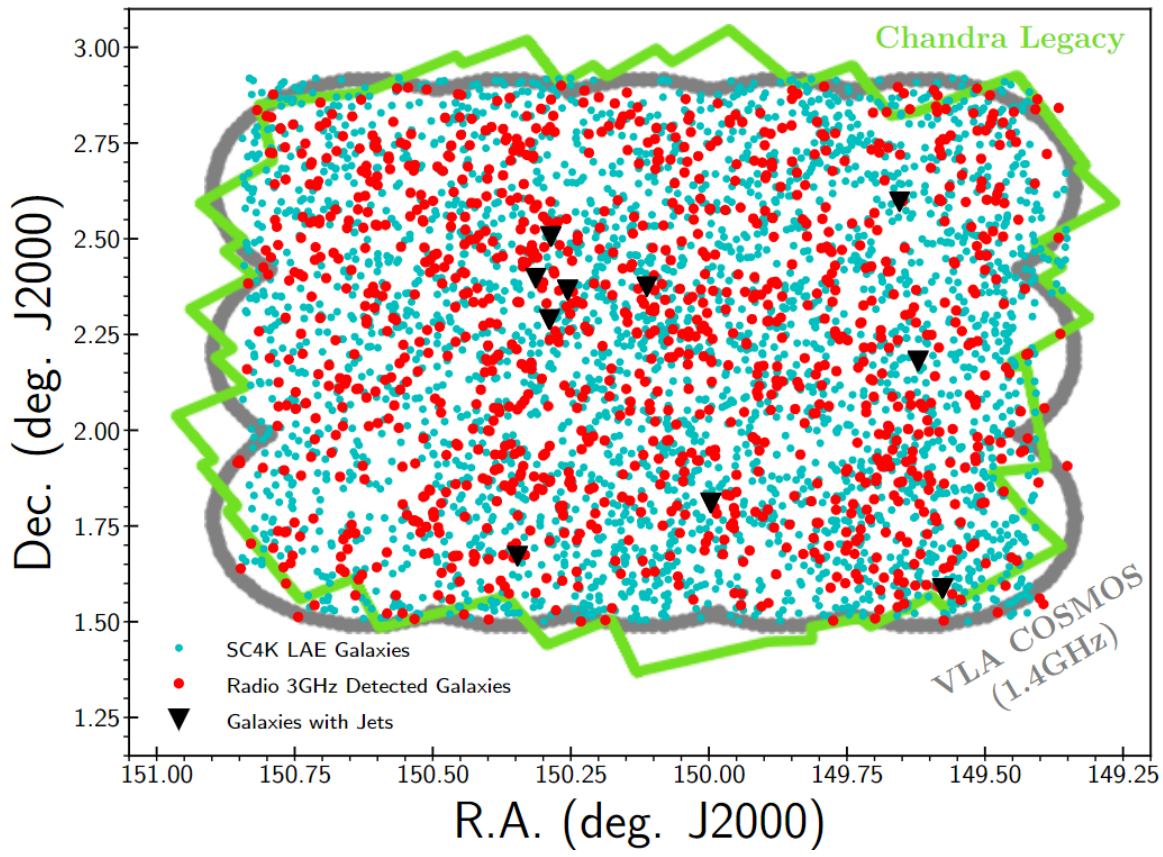

Figure 5. The SC4K LAEs (Sobral et al. 2018) used in this study are shown as small cyan circles. The full radio VLA COSMOS 3GHz catalogue (Smolčić et al. 2017) was used and is represented through the red circles (non-Lyman-alpha emitting radio emissions). The grey boundary illustrates the area covered by the VLA-COSMOS 1.4 GHz survey Schinnerer et al. (2004), and the *Chandra* COSMOS Legacy Civano et al. (2016) survey's green boundary combined gave us 4861 data points. Finally, sources we detected and identified from these as possessing jets are marked with a black triangles, of which there are 10.

Soft, Hard and Full band conversion factors as 0.687, 3.05, and 1.64 respectively. However, for the full flux we perform a translation via an aperture correction seen below:

$$\log_{10}(\mathrm{F_X}) = \log_{10}(\mathrm{F_{X_0}}) + \mathrm{A_C} \tag{3}$$

As we used the same method as Calhau et al. (2020) we used the same aperture correction, thus we find A_C=0.1 and define our full flux F_X.

3.3.4 *Hardness Ratio*

Comparing the soft and hard band and their respective count rates provides a measure of the obscurity of an AGN. Here we use the established definition (see Park et al. 2006):

$$HR = \frac{H - S}{H + S} \tag{4}$$

Here, H represents the count rate in the hard band (2-7keV), and S is the count rate in the soft (0.5-2keV) band. As pointed out in Calhau et al. (2020), requiring both hard and soft band detections in calculating the hardness ratio may bias the data set towards more obscure sources, especially in a low count scenario which is the case with our jet focused collection.

3.3.5 *Determining X-ray Luminosity*

We can convert the observed (X-ray) fluxes into respective luminosities as below:

$$\mathrm{L_X} = 4\pi(\mathrm{F_X})\mathrm{d_L}^2(\mathrm{ergs}^{-1}) \tag{5}$$

Here d_L represents the luminosity distance (in cm). The determination of the this is performed using the corresponding redshift in the narrow/medium waveband.

3.3.6 *Band to Rest Frame Conversion*

Using a K-correction factor from Marchesi et al. (2016) to multiply with the observed (X-ray) luminosity, we convert this into the 0.5-10keV rest frame luminosity as below, such that we can use it to obtain the bolometric luminosity. We also need to understand that this does not correct for absorption at the source.

$$\mathrm{L_{0.5-10keV}} = \frac{\mathrm{L_X}(10^{(2-\Gamma)} - 0.5^{(2-\Gamma)})}{(\mathrm{E_{max}}(1+\mathrm{z}))^{(2-\Gamma)} - (\mathrm{E_{min}}(1+\mathrm{z}))^{(2-\Gamma)})} \tag{6}$$

Here Γ is the photon index, which as in Calhau et al. (2020) we will assume to be 1.4 due to its good average X-ray slope for a population that contains AGN with a variety of obscurity, assuming galactic absorption (Markevitch et al. 2003).

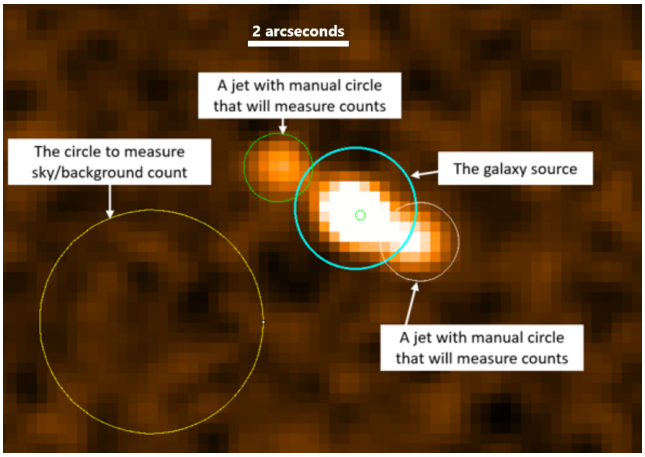

Figure 6. Radio 3GHz image of the COSMOS2015 VLA-311 source in Gaia software (0.2" per pixel, jet aperture size 7.772 pixels used) showing the method used to obtain the average flux per pixel of each individual jet source by comparing against a background count.

Not only this but it correlates well with star forming galaxies projected to have a weak X-ray emission as seen in Alexander et al. (2003).

3.3.7 Bolometric Luminosity

Translating the 0.5-10keV luminosities into their bolometric counterparts is the next step towards determining the host BHAR for our sources, and is done as below:

$$\mathrm{L_{bol}} = 22.4 \times \mathrm{L_{0.5-10keV}} \tag{7}$$

The value of 22.4 here represents the bolometric correction factor we are using. As documented in Vasudevan & Fabian (2007), their research found that this factor varies directly with the Eddington ratio of the sources, varying between 15 and 25 for AGN of ratios <0.1, and varying from 40-70 for those with greater than 0.1. Given this highly varying nature of bolometric corrections, we use the median value (22.4) of those for AGN of $\mathrm{L_X} = 10^{41} - 10^{46}\mathrm{ergs^{-1}}$ (Lehmer et al. 2013; Calhau et al. 2020).

3.3.8 Estimating BHAR

Finally we can calculate our respective BHARs, and do so as below, making a note to account for uncertainty especially stressing and reminding that the value of the bolometric correction is highly variable.

$$\dot{\mathrm{M}}_{\mathrm{BH}} = \frac{\mathrm{L_{bol}}(1-\epsilon)}{\epsilon \mathrm{c}^2} \times 1.59 \times 10^{-30} (\mathrm{M_\odot yr^{-1}}) \tag{8}$$

Here, $\dot{\mathrm{M}}_{\mathrm{BH}}$ is the black hole accretion rate in $M_\odot \mathrm{yr}^{-1}$, c is the speed of light in ms^{-1} and we assume ϵ, the accretion efficiency, to be 0.1 (as in Marconi et al. 2004). While we likewise use the median value for the bolometric correction, Calhau et al. (2020) also points out that in their case, varying this between 15 and 50 results in the BHAR uncertainty being of the order $^{+0.5}_{-0.03}\mathrm{M_\odot yr^{-1}}$. For us however, performing the same variation the mean discrepancy between the values we used and the varied results was $^{+0.1}_{-0.03}\mathrm{M_\odot yr^{-1}}$ with 97% of the results within the range $^{+0.54}_{-0.14}\mathrm{M_\odot yr^{-1}}$.

3.4 Far-Infrared Analysis

Infrared wavelength analysis is used mainly for our focus on the calculation of star formation rates of galaxies with and without jets to observe how jet formation and production may produce an effect if any. The infrared waveband can also be used to identify potentially red-shifted visible wavelengths to confirm or deny the presence of galaxies when carrying out the preliminary observations to investigate and identify the presence of jets in a galaxy source.

3.4.1 Infrared flux Calculation

Apertures of 5"(2.5" radius) were placed over the AGN source such that the whole source was covered, using concentric larger apertures a background count was measured and the result gives a measurement of flux density in mJy/beam. We use the conversion

$$1[\mathrm{Jy/beam}] = 10^{-23}[\mathrm{ergs^{-1}cm^{-2}Hz^{-1}}] \tag{9}$$

on our Infrared fluxes to then enter them into Equation 10.

$$L_{IR}[\mathrm{ergs^{-1}}] = 4 \times \pi \times F_{IR}[\mathrm{ergs^{-1}cm^{-2}}] \times dL^2[\mathrm{cm^2}] \tag{10}$$

where in this case IR=24μm such when integrating flux density to flux, the frequency is ν=1.25×10^{13}Hz.

3.4.2 Estimating Star Formation Rate from Infrared Luminosity

As discussed in Smolčić et al. (2017), the far-infrared (20μm-350μm) is actually the best waveband when it comes to calculating a value for the SFR of a galaxy, above both radio and X-ray. This is because in normal disk galaxies, the relationship between the far infrared (FIR) luminosity and the SFR can be complex due to stars of a variety of ages contributing to the dust heating, and only a fraction of the bolometric luminosity of young stellar objects (YSOs) being absorbed by dust. However, in the starbursts studied Kennicutt (1998), the physical coupling between the SFR and the IR luminosity is much more direct. Young stars dominate the radiation field responsible for heating the dust, and the optical depths are so large that vast majority of the bolometric luminosity (of the starburst) is re-radiated in the infrared.

We used the formula below in order to use and convert our infrared luminosities into the SFR of the host galaxy. This method was documented in Vutisalchavakul & Evans (2013) and derived for extra-galactic star formation, where individual YSOs are not resolved, expecting the detected flux to be contributed from diffuse emission as well as from point sources.

$$\mathrm{SFR}[\mathrm{M_\odot yr^{-1}}] = 1.27 \times 10^{-38} \times (\nu \times \mathrm{L_{24\mu m}}[\mathrm{ergs^{-1}}])^{0.8850} \tag{11}$$

where ν is the detected emission frequency and $L_{24\mu m}$ is the infrared luminosity.

3.5 Determining similar properties for non-jet sources

For sources without jets we could only generate X-ray based data easily. This was done by first generating a list of 1000 random sources which were split between the SC4K and VLA COSMOS datasets proportionally, with respect to our jets (i.e. a 40/60 split between SC4K and VLA COSMOS). Using these sources we performed the X-ray analysis as described in section 3.3. Producing luminosity and accretion rate data. This ran into the problem that as the VLA images were not aligned with the Chandra exactly and the outer regions of the Chandra images were less accurate than the central areas, there were 172 VLA sources which had 0 counts in at least one of the 3 X-ray bands and therefore had to be removed from the dataset, this left us with 828 sources from which we did not detect any jets, making our sample.

3.6 Estimating Effects on Habitability of Nearby Planetary Systems

To estimate the flux of the jets we measured, a number of assumptions had to be made about them.

(i) The entire energy output of all the jets was being emitted in radio frequencies.
(ii) The opening angle of all the jets was 0.01 radian as described in Livio (1997).
(iii) All the particles within the jets were relativistic electrons.

This allowed us to calculate a minimum flux for the jets at various distances and their effect on the habitability of any planets which passed through the body of the jet at various distances.

3.6.1 Estimating Jet Flux

To calculate the flux of the jets we modeled them as a cone with the point at the center of the AGN. Then the flux could be calculated by dividing the total radio luminosity of the jet by the area of the cone at the distance any given distance up to $\sim 10^6$ Pc. This was performed using

$$F_J(d) = \frac{L_\nu}{(0.01 \times d)^2} \tag{12}$$

where F_J is the flux of the jet, L_ν is the radio luminosity of the bulb of the jet, 0.01 is the opening angle, and d is the distance from the source of the jet. However, if we detected two jets being produced by the AGN being analysed then the jet with the largest radio output would be used. This is due to the AGN producing two identical jets initially, therefore if one is more luminous than the other this must be due to it losing energy elsewhere which the other does not.

3.6.2 Calculating radiation effects

To calculate the effects of this flux as radiation we had to compare it to other sources of radiation with known fluxes and effects. As those results were in sieverts we had to convert them into an equivalent energy flux using

$$F_R = \frac{M \times D}{A} \times Q \tag{13}$$

where F_R is the energy flux of the radiation, M is the mass of the body absorbing the radiation, D is the radiation dose in sieverts per second, A is the area of the body and Q in the quality factor, which accounts for the fraction of the energy that is actually absorbed by the body, in our case Q is equal to 1 as we are treating all the particles as electrons (ICRP 2007).

4 RESULTS

Using the method described in section 3.1 we identified 10 AGN which were the source of jets we could investigate further, at a redshift $z \sim 2.2 - 3.5$. Of these jets, 4 were SC4K LAEs and 8 were in the VLA radio catalogue, accounting for 2 sources which were in both catalogues (in SC4K as SC4K-IA484-111739 and SC4K-IA427-26216 and in the VLA radio catalogue as COSMOS2015-229 and COSMOS2015-1728, we used the SC4K name to refer to them in the rest of this paper).

This leads us to determine that of the 2939 LAEs in SC4K with $2.2 < z < 3.5$, $\frac{4}{2939} = 0.13 \pm 0.04\%$ of them have jets and in the population of radio sources there are $\frac{8}{1134} = 0.71 \pm 0.08\%$ which produce jets. The errors are calculated by accounting for the possibility of an AGN with a jet not being identified correctly from the sources, or an incorrect identification of one of the AGN with jets in our determined sample, so we give a ± 1 parameter to the overall number of sources in our sample.

4.1 Jet Parameters

Analysing the X-ray and radio emissions of the AGN and their jets (using the method detailed in sections 3.2 and 3.3) we determine that the jets have an average radio luminosity of $2.272 \pm 0.010 \times 10^{25}$ W Hz^{-1} in the 3GHz band and $3.104 \pm 0.014 \times 10^{25}$ W Hz^{-1} in the 1.4GHz band. The average accretion rate of the AGNs producing these jets is $0.141^{+0.078}_{-0.016}$ M$_\odot$yr^{-1} with and average X-ray hardness of 0.26. The average star formation rate of the source galaxies producing the jets is 92.0±2.11 M$_\odot$yr^{-1} but varies between 352±8.14 and 9.13 M$_\odot$yr^{-1}. For more detailed data see Table 1 for individual jets and Table 2 for the galaxies producing the jets.

4.2 Comparison

Using the method described in section 3.5 we collected usable data from 828 AGN without jets: 400 from the SC4K sample of LAEs (Sobral et al. 2018) and 428 from the VLA radio catalogue (Smolčić et al. 2017).

4.2.1 Luminosity

Figure 8 shows that the average X-ray luminosity of AGN that produce jets is 6.72×10^{43}erg s^{-1} which is lower than

Table 1. The radio data of our ten identified jet sources, six of which had two distinguished jets which also needed analysing individually (included in the same row as their partner), giving us a total of 16 entries. We did not determine uncertainties in the redshifts, though as outlined in Sobral et al. (2018) it is possible to do so using the NB or MB filter widths. The fluxes are determined following the process explained in Section 3.2, using circular apertures ranging from 1.4" to 4.6" (see Section 3.2.2) and making them comparable to Smolčić et al. (2017).

Identification	RA (HH:MM:SS)	DEC (Deg:MM:SS)	Redshift	F_{3GHz} (μJy)	$\log_{10}(L_{3GHz})$ (W Hz^{-1})	$\log_{10}(L_{1.4GHz})$ (W Hz^{-1})
SC4K-IA427-26216	10:01:15	+02:23:50	2.51	68.57 ± .79	24.427 ± 0.005	24.631 ± 0.010
SC4K-IA464-75921	09:58:29	+02:10:52	2.82	55.14 ± .58	24.446 ± 0.005	24.667 ± 0.021
SC4K-IA464-75921	09:58:29	+02:10:52	2.82	54.82 ± .95	24.443 ± 0.007	24.611 ± 0.018
SC4K-IA484-111739	09:58:37	+02:35:49	2.98	750.00 ± 9.37	25.635 ± 0.005	26.002 ± 0.001
SC4K-IA484-33705	10:01:01	+02:21:59	2.98	298.47 ± 5.97	25.235 ± 0.009	25.087 ± 0.003
SC4K-IA484-3	10:01:01	+02:21:59	2.98	47.03 ± .94	24.432 ± 0.009	25.057 ± 0.004
COSMOS2015-89	10:01:09	+02:17:22	2.58	1154.50 ± 1.99	25.681 ± 0.001	25.629 ± 0.001
COSMOS2015-89	10:01:09	+02:17:22	2.58	1670.44 ± 1.84	25.841 ± 0.001	25.987 ± 0.001
COSMOS2015-311	09:58:18	+01:35:14	2.45	58.46 ± 1.33	24.334 ± 0.010	25.600 ± 0.002
COSMOS2015-311	09:58:18	+01:35:14	2.45	362.28 ± 1.19	25.126 ± 0.001	25.587 ± 0.002
COSMOS2015-3477	10:00:27	+02:22:31	2.21	81.14 ± 1.62	24.372 ± 0.009	24.545 ± 0.013
IRAC-3528	10:01:09	+02:30:23	2.22	17.83 ± .36	23.718 ± 0.009	24.699 ± 0.007
IRAC-3528	10:01:09	+02:30:23	2.22	25.73 ± .51	23.877 ± 0.009	24.698 ± 0.007
iband-5172	10:01:23	+01:40:17	2.63	13.66 ± 1.24	23.773 ± 0.038	24.028 ± 0.047
COSMOS2015-10915	09:59:59	+01:48:38	2.36	1493.28 ± 2.30	25.702 ± 0.001	25.637 ± 0.001
COSMOS2015-10915	09:59:59	+01:48:38	2.36	3104.53 ± 2.46	26.020 ± 0.001	25.920 ± 0.002

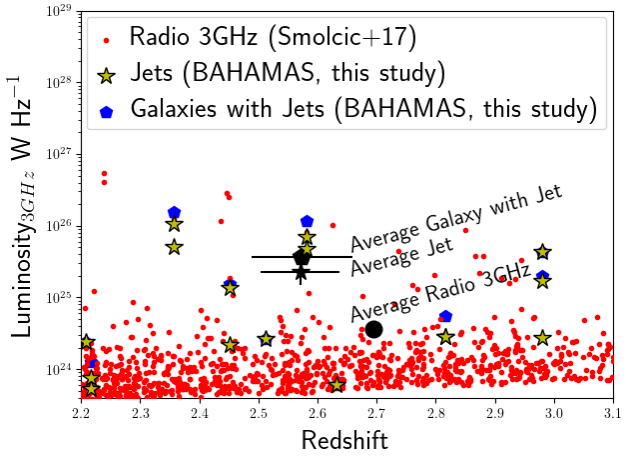

Figure 7. The radio 3GHz Luminosity of jets and the total luminosity of galaxies with jets, compared to galaxies without jets at different redshifts. It shows that on average, jets and galaxies with jets, are brighter than the average radio emitting galaxy with no jets.

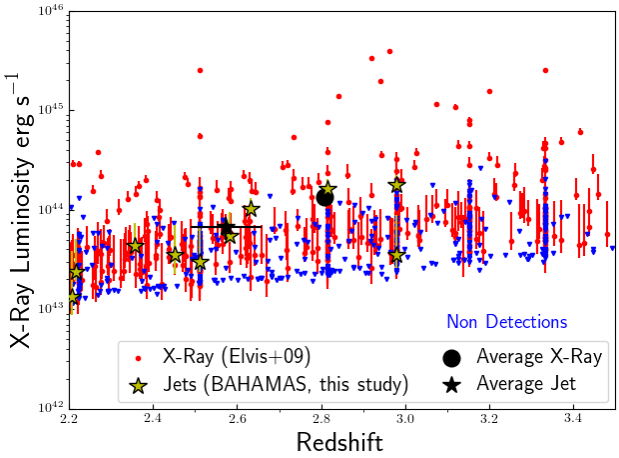

Figure 8. The relation between X-Ray luminosity and redshift for AGN with and without jets. The average X-ray emission from AGN producing jets are lower than the average of the AGN without jets detected with a S/N > 3

the average for AGN, with a signal to noise ratio > 3, that do not produce jets of 1.329×10^{44}erg s^{-1}. It also shows that the X-ray emission from AGN with jets increases with redshift more than AGN without jets, indicating that the X-ray emissions have been dropping in galaxies with jets faster than in those galaxies without them.

4.2.2 Star Formation Rate

The average SFR for AGN with jets was calculated to be $92.0 \pm 2.11 M_{\odot} yr^{-1}$ whereas the average SFR for AGN without jets was found to be $274 \pm 8.14 M_{\odot} yr^{-1}$. These values are calculated for the redshift range $2.2 < z < 3.5$. By comparison Barlow-Hall et al. (2019) obtained an average SFR of $\sim 17 M_{\odot} yr^{-1}$. This was however taken between the range $2 < z < 6$ which explains the large discrepancy between

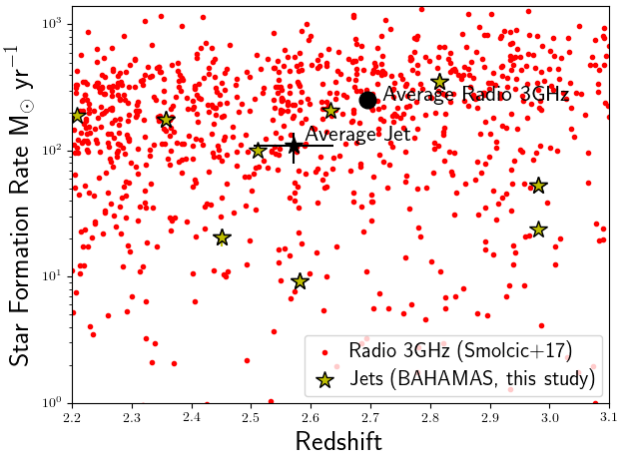

Figure 9. A comparison of the star formation rate (SFR) in galaxies with and without jets. Our results show the average SFR in the galaxies without jets is $\sim 3\times$ that of the the average of the SFR in the galaxies, without showing any obvious impact of jets on SFR

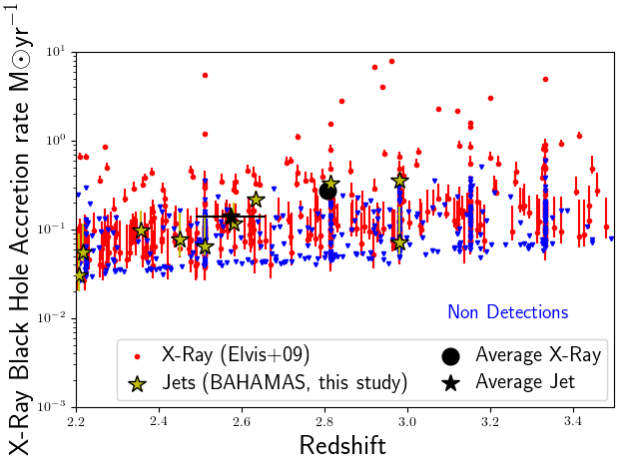

Figure 11. The relationship between the black hole accretion rate in galaxies with and without jets. This shows that the average accretion rate of both the jetted and non-jetted sources increases with redshift showing that the BHAR has no obvious impact on the presence of jets.

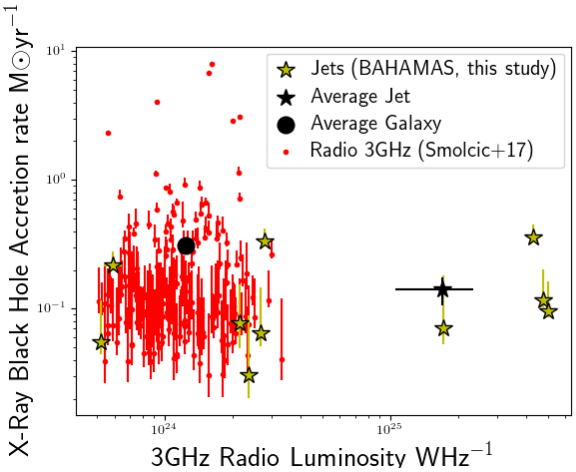

Figure 10. The relationship between the radio luminosity of the individual jets and the black hole accretion rate of the galaxies producing our jets. This shows that the average accretion rate for the AGNs we have found that produce jets is lower than the average accretion rate for the galaxies without jets

our results. This suggests that the SFR within high redshift sources is significantly lower such that is brings the average down. We conclude that our results are statistically significant due to our results having small errors that would not alter our results or conclusions if applied, showing that the presence of jets in AGN affects the SFR by inhibiting it.

4.2.3 Accretion Rate

Figure 10 appears to have two distinct lines of correlation for the jetted sources which occur when the BHAR is between $0.2 - 0.3 M_\odot yr^{-1}$ and $0.05 - 0.1 M_\odot yr^{-1}$. Therefore it appears some jetted sources have a BHAR that is $2 - 3$ times as large as other jetted sources. It is also clear to see there is a slight increase in the X-ray BHAR with increasing radio luminosity. This Figure also suggests that on average AGN without jets have a greater BHAR than AGN with jets. The average accretion rate of a galaxy without jets is approximately $0.271^{+0.091}_{-0.019} M_\odot yr^{-1}$ in contrast to the relatively small average accretion rate of $0.141^{+0.078}_{-0.016}$ $M_\odot yr^{-1}$ for jetted sources.

Figure 11 shows that there is a gradual increase in the BHAR for both jetted and non-jetted sources. There are significantly more AGNs with high accretion rates at $z > 2.7$. The clear absence of jet detections when $z > 3$ can also be clearly in this Figure.

4.2.4 X-ray hardness

As shown in Figure 12 the galaxies with jets with a redshift of less than 2.9 have an average hardness of 0.41 ± 0.21 which is considerably higher than the average of the galaxies without jets which is 0.14 ± 0.47. However, the two jets at redshift 2.98 both have X-ray hardnesses below 0.0.

4.3 Impact of jets on habitability

Using the method outlined in section 3.6 we can calculate the flux of the jets as a function of distance and compare them to known radiation sources. From this we can calculate that the radiation levels start to become non-negligible at 10^{-9} Wm^{-2} closer than 10^6 AU from the AGN, where it approaches the global background radiation level of 3.01 mSv yr^{-1} (UNSCEAR 2008). As any planets approach at closer distances the radiation levels increase to the limit for a nuclear worker of 50 mSv yr^{-1} (USNRC 2018), equivalent to 2×10^{-5} Wm^{-2} at between 2×10^4 to 2×10^5 AU. At a distance of between 2 and 20 AU the radiation rises to 530 Sv h^{-1} or 20 Wm^{-2} these are the levels found inside a nuclear reactor (TEPCO 2017) and at distances closer that ~ 1 AU

Table 2. X-ray data we obtained, with entries being the same jet sources as Table 1 though with only the 10 rows due to the X-ray detection being from the host AGN. The X-ray luminosities were estimated from the full band fluxes, which were in turn taken from the 0.5 - 10 keV *Chandra* Legacy survey images. We also present the BHARs we calculated from the X-ray luminosities of our sources (see Section 3.3.8). The full SC4K catalogue (Sobral et al. 2018) used initially before the inclusion of VLA-COSMOS, includes LAEs detected and undetected in the X-rays, as well as their radio, FIR and Lyα properties. The SFR was estimated as detailed in Section 3.4.2, with the one missing source (IRAC-3528) as it just so happened the Spitzer infra-red telescope did not cover it, thus there is no FIR cutout to calculate the SFR from.

Identification	RA (HH:MM:SS)	DEC (Deg:MM:SS)	Redshift	$\log_{10}(L_{x-ray})$ (W Hz^{-1})	Accretion Rate (M$_\odot$yr^{-1})	SFR (M$_\odot$yr^{-1})
SC4K-IA427-26216	10:01:15	+02:23:50	2.51	$43.47^{+0.35}_{-0.083}$	$0.065^{+0.081}_{-0.014}$	99.75±3.99
SC4K-IA464-75921	09:58:29	+02:10:52	2.82	$44.20^{+0.10}_{-0.02}$	$0.331^{+0.088}_{-0.017}$	352±8.77
SC4K-IA484-111739	09:58:37	+02:35:49	2.98	$44.24^{+0.10}_{-0.23}$	$0.355^{+0.094}_{-0.019}$	23.62±1.47
SC4K-IA484-33705	10:01:01	+02:21:59	2.98	$43.55^{+0.40}_{-0.10}$	$0.071^{+0.109}_{-0.019}$	52.53±2.92
COSMOS2015-89	10:01:09	+02:17:22	2.58	$43.73^{+0.24}_{-0.05}$	$0.117^{+0.086}_{-0.014}$	9.13
COSMOS2015-311	09:58:18	+01:35:14	2.45	$43.55^{+0.30}_{-0.13}$	$0.077^{+0.078}_{-0.028}$	20.38
COSMOS2015-3477	10:00:27	+02:22:31	2.21	$43.12^{+0.46}_{-0.13}$	$0.031^{+0.059}_{-0.010}$	189.35
IRAC-3528	10:01:09	+02:30:23	2.22	$43.38^{+0.32}_{-0.76}$	$0.055^{+0.061}_{-0.010}$	-
iband-5172	10:01:23	+01:40:17	2.63	$44.01^{+0.11}_{-0.04}$	$0.216^{+0.061}_{-0.019}$	205.70
COSMOS2015-10915	09:59:59	+01:48:38	2.36	$43.63^{+0.23}_{-0.05}$	$0.096^{+0.067}_{-0.011}$	174.84

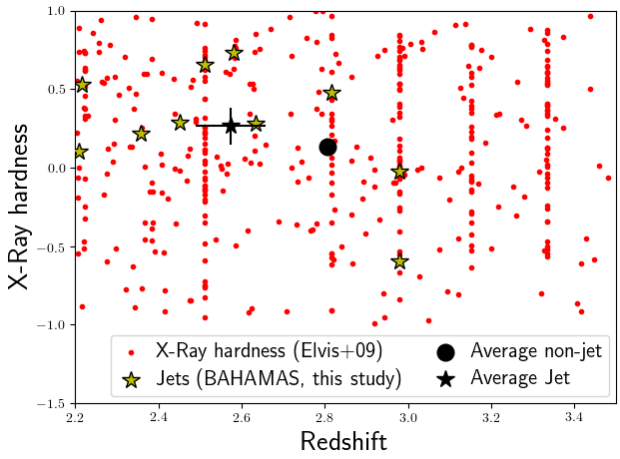

Figure 12. A comparison of the hardness of the X-ray emissions from sources with and without jets. It can be seen that the for sources without jets the hardness varies smoothly between -1 and 1. However for the sources with jets all the sources closer than z $\approx$ 2.9 are greater than 0 and it is only the two sources with redshift $>$ 2.9 that have a hardness less than 0

where the flux is $\sim$ 1000 Wm^{-2} a human would experience a fatal dose of radiation (8 Sv s^{-1} (Bushberg 2019)) in $<$1s (see Figure 13)

5 DISCUSSION

In the following sections we will investigate the potential causes of jet formation and the effects that jets have on their environment, concluding on our comparisons made between jetted and non-jetted sources in section 4.2.

5.1 Influence of environment on jet formation and detection

5.1.1 Impact of BHAR on jet formation

The graph of the BHAR against the radio luminosity of the jet lobes in Figure 10 appears to show two lines of positive correlation which could be potentially associated with the jetted AGN having varying accretion flows (see Abramowicz & Fragile 2013). As discussed in section 4.2.3 there appears to be good correlation between the radio luminosity of the lobes and the BHAR which suggests that this could potentially be an influencing factor in powering jets. This agrees with the work of Ghisellini & Celotti (2001) which then leads to the suggestion that the difference in jet structures of FR-I and FR-II jets is due to the jet velocity. The slower FR-I jets would be susceptible to shearing instabilities (King et al. 2015) unlike the faster FR-II type jets. The graph also suggests that both of the accretion modes could potentially result in high powered jets.

In contrast to this, it is clear to see from Figure 11 that the BHAR is increasing as redshift increases implying that that the rate of black hole growth appears to be slowing down with time. This trend appears to be replicated for the jetted and non-jetted sources which implies that the presence of jets has no influence on the BHAR and likewise the BHAR has no influence on the presence of jets. It could also be suggested from this that there may be multiple factors influencing the presence of jets.

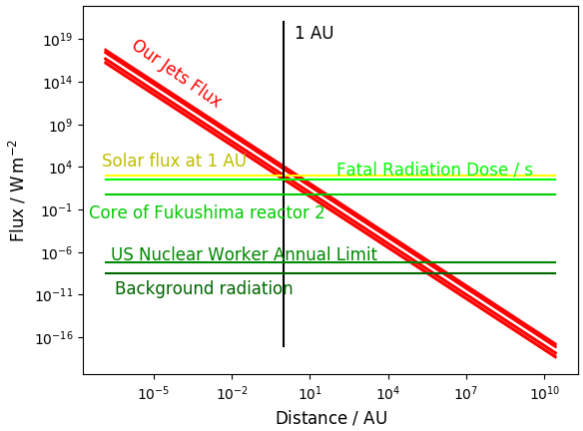

Figure 13. The flux from the ten jets we have detected (shown in red) plotted against distance in AU. Also shown for comparison is the flux of several known radiation sources. These are (from lowest to highest) the global background radiation level of 3.01 mSv yr^{-1} (UNSCEAR 2008), the US nuclear worker annual limit of 50 mSv yr^{-1} (USNRC 2018) spread over a year, the flux in the core of Fukushima reactor 2 in Feb 2017 of (530 Sv h^{-1}) (TEPCO 2017) and the flux which would cause a fatal radiation dose to a human in 1 second (8 Sv s^{-1}) (Bushberg 2019). This is also compared to the flux of the Sun at 1 AU. Showing the output of these jets could have a large effect on the habitability of a planetary system which passed through the jet within 10^5 AU $\approx$ 1 Pc of the AGN.

5.1.2 Impact of radio luminosity on jet formation

We have also found from Figure 7 that the average radio luminosity of the galaxies with jets are significantly greater than the average 3GHz radio luminosity for the galaxies without jets. This suggests that powerful jets are produced from mainly radio-loud AGNs which is in agreement with Livio (1997). Livio (1997) suggest that there could be several potential explanations as to why this relationship is observed. Firstly, if the central engine used to accelerate and collimate jets is the same within radio-loud and radio-quiet AGNs then it can be assumed that there is an external factor within the radio-quiet AGN that inhibits jet formation. Blandford & Levinson (1995) suggested that this external factor could occur when the central density of mass-losing stars is large which results in the the hydromagnetic wind being unable to collimate jets. Alternatively, Fabian & Rees (1995) proposed that the absence of a hot atmospheres will result in the mechanism for collimation of jets being halted. These hot atmospheres are found to be present in elliptical galaxies and as Wilson & Colbert (1995) found these galaxies are mainly host to radio-loud objects such as AGNs whereas spiral galaxies are mainly found to contain radio-quiet objects. Therefore, we can say with a slight scepticism that jets are mainly produced from radio-loud AGNs within elliptical galaxies. This conclusion however could be influenced by our observational bias as we can only detect jetted sources that are highly luminous. In addition, the small sample size for jetted sources reduces our confidence in this conclusion. As mentioned previously and within other research we have found that jets are likely to have a significant impact on their environment and we have seen evidence from our results in section 4.2.2 that suggests the possibility of jets influencing the SFR within the galaxy. However, from the supporting evidence that our results provide to the theories proposed by Fabian & Rees (1995) and Blandford & Levinson (1995) we can suggest that jets are also heavily influenced by the environment they are within. We suggest from these results that there may be several factors involved in causing jet formation and also conclude that if the environment is not suitable then jets will not form.

5.1.3 Impact of CMB induced radio-quenching on jet detection

The graphs of X-ray (Figure 8) and radio luminosity (Figure 7) against redshift appear to show that the radio luminosity decreases with redshift for jetted sources and the X-ray luminosity appears to increase for jetted and non-jetted sources as redshift increases. In addition, these graphs also demonstrate the absence of jet detections at $z > 3$. These observed trends support the theory of cosmic microwave background (CMB) induced radio quenching proposed by Wu et al. (2017). The theory suggests that at $z \sim 3$ the CMB energy density described by the $(1+z)^4$ dependence becomes equivalent to the magnetic energy density. This results in the suppression of synchrotron radiation at $z > 3$ as the high energy electrons within the jet cool through an inverse Compton scattering interaction with CMB photons. Ultimately, there is an increase in the X-ray radiation emitted and this band appears enhanced relative to the radio band.

5.2 Impact of jets on their local environment

Figure 5 appears to show a clustered region with many jetted sources which originally suggested that the jets from these galaxies could perhaps influence others which supported the theory proposed by Blandford et al. (2019). However, after examining the redshift of these sources it appears they are not clustered. This suggests that our results do not support this theory and instead suggests that jets do not influence other galaxies. However, there are several indications within the results we have obtained which suggest that jets can have an impact on the environment they are in. This will be outlined in the following sections.

5.2.1 Impact of jets on star formation rate

Barlow-Hall et al. (2019) investigated the relationship between the SFR and redshift which we have also done in this study (see Section 4.2.2). They find that the SFR increases with redshift in both the radio, FIR, rest frame UV and Lyα. This however is in contrast with the results obtained by Smit et al. (2012) which suggests that the SFR decreases with increasing redshift. The results we obtain Figure 9 imply that there is little correlation between the SFR and the redshift for jetted sources. Due to there being little correlation this suggests that jetted sources may influence the SFR in their surroundings. This could however be due to the small redshift range of the sources used. This does however agree with the predictions made within Blandford et al. (2019)

that suggest jets can influence the star formation within a galaxy by both stimulating star formation and inhibiting it. The SFR can be stimulated due to the presence of shocks within jets (e.g. van Breugel et al. 2003) due to a moderately dense and warm gaseous environment being created. Blandford et al. (2019) also suggests that not only can star formation be induced within the host galaxy but it can also be induced within other galaxies as jets can extend to several Mpc. From this it is possible to probe the idea that jets can have major influences in galactic clusters. Star formation can be inhibited over a long period of time due to Kelvin-Helmholtz instabilities at the interface between the jet and the interstellar medium. The mass of the cloud will decrease and hence the SFR also decreases as demonstrated in Antonuccio-Delogu & Silk (2008). Section 4.2.2 and Figure 9 imply that the inhibiting effect from Kelvin-Helmholtz instabilities has a more dominant effect on the SFR of the galaxy than the inducing effect from the shocks within jets. This is due to the average SFR for galaxies with jets being less than half the SFR of galaxies without jets.

5.2.2 Impact of jets on BHAR

The more rapid decreases in BHAR from jetted sources (as shown in Figures 8 and 11) could be due to the jets ejecting sizable quantities of the material that the AGN is accreting from, thereby reducing the amount available at a higher rate than those galaxies where the AGN can consume all the available material.

5.2.3 Impact of jets on X-ray hardness

The shift in X-ray hardness at $z \approx 2.9$, as shown in Figure 12, could be due to the presence of the jet. As the peak in AGN activity is at $z \sim 2$ (Wolf et al. 2003; Delvecchio et al. 2014) and we have found no jets earlier than $z = 3$, therefore indicating that the AGNs at $z \sim 3$ have only recently formed and the jets at lower redshift have been around longer allowing them more time for the jet to increase the hardness of the emissions. This could be by either increasing the average velocity of the particles involved in the inverse Compton scattering in the accretion disk thereby increasing the energy of the X-rays or by absorbing more of the lower energy photons and only allowing the higher energy photons to escape.

5.3 Impact of selection bias on results

Despite establishing some clear trends in section 4 it is likely that they are affected by error and selection bias. When initially detecting the jets we were attempting to observe the lobed FR-II jet structure similar to Figure 2. Therefore, we have ultimately obtained mainly FR-II jets within our results due to them being significantly easier to observe. These jets appear to be more luminous in comparison to FR-I type jets and therefore with increasing redshift the likelihood of observing an FR-I type jet becomes rare. When observing jets we have been using the highly luminous radio lobes to identify them however FR-I type jets do not produce lobes, instead having much dimmer plumes which are more difficult to detect. As a result of this selection bias it is very difficult to make conclusions on the distribution of these jet types with redshift and we can only speculate due to the small sample size. Selection bias may have also originated from the projection of the jets relative to our line of sight. Despite viewing the sources in several different wavebands it is difficult to detect jet systems that have relatively small angles to our line of sight hence ruling out a portion of our sample. As a result of this selection bias we can assume that the proportion of galaxies with jets is greater than what we have estimated in Section 4, instead our results represent a lower limit to the number of jetted galaxies.

Our method of detecting jets also required the jets to be at a fairly oblique angle to the observer therefore we would not have detected any jets that were pointing directly towards us. As the higher energy emissions from the jets will be more collimated than the radio emissions, finding some of these jets would be the only way to accurately detect the higher energy emissions from the jets and therefore calculate a more accurate minimum for the flux of the jets along their length than described in Section 4.3.

6 CONCLUSIONS

We have looked for the presence of jets produced by AGNs in LAEs and radio-selected sources at z$\sim 2.2-3.5$. We have compared properties of the AGNs for jetted and non-jetted sources in an attempt to better understand some of the underlying causes of jet formation. We have also attempted to investigate the effects of jets on their surrounding environment. We have found that:

- Out of a total of over 9,000 sources we have identified 10 jet producing AGN in the COSMOS field with $2.2 < z < 3.5$. Four of them are LAEs with jets, representing $0.13\pm0.04\%$ of the LAE population and 8 are radio-selected galaxies with jets representing $0.71\pm0.08\%$ of the population, with 2 galaxies in both sets.
- The average radio luminosity of the jets is $2.272 \pm 0.010 \times 10^{25}$ W Hz^{-1} in the 3GHz band and $3.104 \pm 0.014 \times 10^{25}$ W Hz^{-1} in the 1.4GHz band.
- The accretion rate of the AGNs producing these jets averages to $0.141^{+0.078}_{-0.016}$ M$_\odot$yr^{-1} and the star formation rate of these galaxies is varies between 352 ± 8.8 M$_\odot$yr^{-1} and 9.13 M$_\odot$yr^{-1} with an average of 92 ± 2.11 M$_\odot$yr^{-1}.
- The X-ray luminosity and BHAR of the galaxies with jets shows a potential faster decline over time than the galaxies without jets.
- The X-ray hardness of jet producing galaxies with $z < 2.9$ averages to 0.41 ± 0.21, which is considerably higher than that of galaxies without jets of 0.14 ± 0.47, with a sharp drop at $z \approx 3$ where the hardness of the galaxies with jets drops to <0.0.
- The average star formation rate of galaxies with jets is 92.0 ± 2.11M$_\odot$yr^{-1} where galaxies without jets have an average value of 274 ± 8.14M$_\odot$yr^{-1}.
- The BHAR of the galaxies with jets on average, of $0.141^{+0.078}_{-0.016}$ M$_\odot$yr^{-1}, is lower than the average of X-ray detected galaxies, which is $0.271^{+0.091}_{-0.019}$M$_\odot$yr^{-1}.
- The presence of jets in an AGN drastically affects the potential habitability of an planetary system which passes through the jet at any distance < 1 pc.

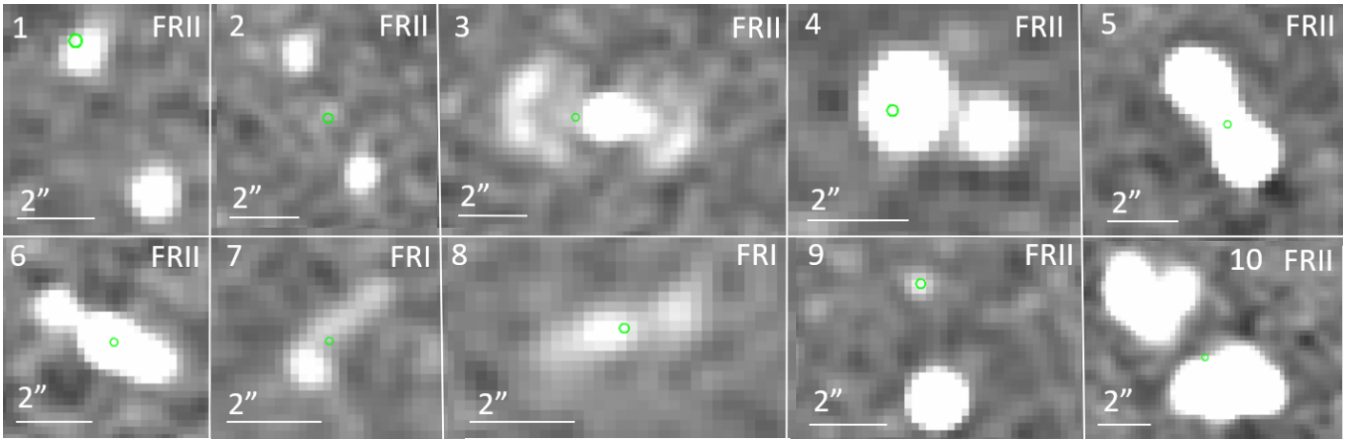

Figure 14. The radio 3GHz jet morphologies of our 10 galaxy data set represented in Table 1 and Table 2, their classification number in the top left of each image with a 2" scale on each image for reference. The morphology classification developed by Fanaroff & Riley (1974) of FR-I and FR-II are included on each galaxy in the top right of each image.

Further work within this field could involve taking spectroscopic measurements of the AGN and the jets they emit in order to determine the mass of the SMBH. This may be carried out through a measurement of the size of the x-ray emitting region to estimate the radius of the central SMBH, and therefore calculate the mass. This would allow an insight into whether the mass of the SMBH is an influencing factor in the presence of jets. This could hence give an insight into whether SMBHs can use jets as a method for influencing their surroundings and the impact this has on the evolution of the galaxy.

ACKNOWLEDGMENTS

This work is based in part on data from the public SC4K sample (Sobral et al. 2018) and the VLA COSMOS radio catalogue (Smolčić et al. 2017). We have benefited immensely from the public available programming language Python, including NumPy & SciPy (Van Der Walt et al. 2011; Jones et al. 2001), Matplotlib (Hunter 2007), Astropy (Astropy Collaboration et al. 2013) and the Topcat analysis program (Taylor 2013).

REFERENCES

Abramowicz M. A., Fragile P. C., 2013, Living Reviews in Relativity, 16, 1
Alexander D. M., et al., 2003, AJ, 125, 383
Allen S. W., Dunn R. J. H., Fabian A. C., Taylor G. B., Reynolds C. S., 2006, MNRAS, 372, 21
Antonuccio-Delogu V., Silk J., 2008, Monthly Notices of the Royal Astronomical Society, 389, 1750–1762
Astropy Collaboration et al., 2013, A&A, 558, A33
Balbus S. A., Hawley J. F., 1998, Rev. Mod. Phys., 70, 1
Barlow-Hall C., Bramwell J., Hodder D., Merrett M., Russ A., Wareing O., Sobral D., 2019, Notices of Lancaster Astrophysics (NLUAstro), 1, 39
Blandford R. D., Levinson A., 1995, ApJ, 441, 79
Blandford R. D., Payne D. G., 1982, MNRAS, 199, 883
Blandford R. D., Znajek R. L., 1977, MNRAS, 179, 433
Blandford R., Meier D., Readhead A., 2019, Annual Review of Astronomy and Astrophysics, 57, 467
Bondi M., Ciliegi P., Schinnerer E., Smolčić V., Jahnke K., Carilli C., Zamorani G., 2008, ApJ, 681, 1129
Bushberg J. T., 2019, Radiation Exposure and Contamination, https://www7.tepco.co.jp/newsroom/announcements/archives/2017/1374451_10494.html
Calhau J., et al., 2020, Monthly Notices of the Royal Astronomical Society
Capak P., et al., 2007, ApJS, 172, 99
Celotti A., Padovani P., Ghisellini G., 1997, Monthly Notices of the Royal Astronomical Society, 286, 415–424
Civano F., et al., 2016, The Astrophysical Journal, 819, 62
Croston J., Ineson J., Hardcastle M., 2018, Monthly Notices of the Royal Astronomical Society, 476, 1614
Delhaize J., et al., 2017, A&A, 602, A4
Delvecchio I., et al., 2014, MNRAS, 439, 2736
Elvis M., et al., 2009, ApJS, 184, 158
Fabian A. C., Rees M. J., 1995, MNRAS, 277, L55
Fanaroff B. L., Riley J. M., 1974, MNRAS, 167, 31P
Geach J. E., Smail I., Best P. N., Kurk J., Casali M., Ivison R. J., Coppin K., 2008, MNRAS, 388, 1473
Ghisellini G., Celotti A., 2001, A&A, 379, L1
Ghisellini G., Tavecchio F., Foschini L., Ghirlanda G., Maraschi L., Celotti A., 2009, Monthly Notices of the Royal Astronomical Society, 402, 497–518
Ghosh P., Abramowicz M. A., 1997, MNRAS, 292, 887
Haardt F., Maraschi L., 1991, ApJ, 380, L51
Hunter J. D., 2007, Computing In Science & Engineering, 9, 90
ICRP 2007, Ann. ICRP, 37
Jones E., Oliphant T., Peterson P., et al., 2001, SciPy: Open source scientific tools for Python, http://www.scipy.org/
Kennicutt Robert C. J., 1998, ApJ, 498, 541
King A. L., Miller J. M., Bietenholz M., Gültekin K., Reynolds M., Mioduszewski A., Rupen M., Bartel N., 2015, The Astrophysical Journal, 799, L8
Le Floc'h E., et al., 2009, The Astrophysical Journal, 703, 222–239
Lehmer B. D., et al., 2013, ApJ, 765, 87
Livio M., 1997, International Astronomical Union Colloquium, 163, 845–866
Loeb A., Rasio F. A., 1994, ApJ, 432, 52
Madau P., Rees M. J., 2001, ApJ, 551, L27
Marchesi S., et al., 2016, ApJ, 827, 150
Marconi A., Risaliti G., Gilli R., Hunt L. K., Maiolino R., Salvati M., 2004, MNRAS, 351, 169

Markevitch M., et al., 2003, ApJ, 583, 70
McKinney J. C., Tchekhovskoy A., Blandford R. D., 2013, Science, 339, 49
Mezcua M., 2017, International Journal of Modern Physics D, 26, 1730021
Mezcua M., Civano F., Marchesi S., Suh H., Fabbiano G., Volonteri M., 2018, MNRAS, 478, 2576
Narayan R., McClintock J. E., 2013, Observational Evidence for Black Holes (arXiv:1312.6698)
Padovani P., 2017, Frontiers in Astronomy and Space Sciences, 4
Park T., Kashyap V. L., Siemiginowska A., van Dyk D. A., Zezas A., Heinke C., Wargelin B. J., 2006, ApJ, 652, 610
Penrose R., Floyd R. M., 1971, Nature Physical Science, 229, 177
Sanders D. B., et al., 2007, ApJS, 172, 86
Schinnerer E., et al., 2004, The Astronomical Journal, 128, 1974
Schinnerer E., et al., 2007, ApJS, 172, 46
Schinnerer E., et al., 2010, ApJS, 188, 384
Scoville N., et al., 2007, ApJS, 172, 1
Smit R., Bouwens R. J., Franx M., Illingworth G. D., Labbé I., Oesch P. A., van Dokkum P. G., 2012, The Astrophysical Journal, 756, 14
Smolčić V., et al., 2017, A&A, 602, A1
Sobral D., et al., 2009, MNRAS, 398, 75
Sobral D., Smail I., Best P. N., Geach J. E., Matsuda Y., Stott J. P., Cirasuolo M., Kurk J., 2013, MNRAS, 428, 1128
Sobral D., et al., 2017, in prep
Sobral D., Santos S., Matthee J., Paulino-Afonso A., Ribeiro B., Calhau J., Khostovan A. A., 2018, MNRAS, 476, 4725
Spruit H. C., 1996, Magnetohydrodynamic winds and jets from accretion disks (arXiv:astro-ph/9602022)
TEPCO 2017, Investigation inside the pedestal for Unit 2 Primary Containment Vessel at Fukushima Daiichi Nuclear Power Station, https://www7.tepco.co.jp/newsroom/announcements/archives/2017/1374451_10494.html
Taylor M., 2013, Starlink User Note, 253
Torres-Albà N., Bosch-Ramon V., Iwasawa K., 2020, Astronomy & Astrophysics, 635, A57
UNSCEAR 2008, UNSCEAR 2008 REPORT Vol. I. United Nations
USNRC 2018, NCR: 10 CFR 20.1201 Occupational dose limits for adults., https://www.nrc.gov/reading-rm/doc-collections/cfr/part020/part020-1201.html
Van Der Walt S., Colbert S. C., Varoquaux G., 2011, Computing in Science & Engineering, 13, 22
Vasudevan R. V., Fabian A. C., 2007, MNRAS, 381, 1235
Vutisalchavakul N., Evans Neal J. I., 2013, ApJ, 765, 129
Wilson A. S., Colbert E. J. M., 1995, ApJ, 438, 62
Wolf C., Wisotzki L., Borch A., Dye S., Kleinheinrich M., Meisenheimer K., 2003, A&A, 408, 499
Wu J., Ghisellini G., Hodges-Kluck E., Gallo E., Ciardi B., Haardt F., Sbarrato T., Tavecchio F., 2017, Monthly Notices of the Royal Astronomical Society, 468, 109–121
van Breugel W., Fragile C., Anninos P., Murray S., 2003, Jet-Induced Star Formation (arXiv:astro-ph/0312282)

APPENDIX A: JET MORPHOLOGIES

The Jet morphologies and their classifications can be seen in Figure 14.

This paper has been typeset from a TEX/LATEX file prepared by the author.